Dispersive shock waves with nonlocal nonlinearity

Christopher Barsi, Wenjie Wan, Can Sun, and Jason W. Fleischer*

Department of Electrical Engineering, Princeton University, Princeton, New Jersey 08544, USA
**Corresponding author: jasonf@princeton.edu*

Received July 13, 2007; revised August 15, 2007; accepted August 21, 2007;
posted August 22, 2007 (Doc. ID 85235); published October 3, 2007

We consider dispersive optical shock waves in nonlocal nonlinear media. Experiments are performed using spatial beams in a thermal liquid cell, and results agree with a hydrodynamic theory of propagation. © 2007 Optical Society of America

OCIS codes: 190.4420, 190.4870.

Dispersion plays many roles in nonlinear optics, as the relative propagation of modes can either enhance or counteract the effects of mode coupling. Examples range from the balance of linear and nonlinear phase shifts in soliton formation [1] to radiative decay and supercontinuum generation [2]. Recently, the spatial equivalent of dispersion, i.e., diffraction, was used with defocusing nonlinearity to form dispersive shock waves in spatial beams [3]. Unlike dissipative shock waves, which have a thin, well-defined front due to energy absorption (e.g., viscosity), dispersive shock waves have a wavefront characterized by oscillations. In this case, dispersion and nonlinearity act in the same direction, creating a front profile resembling a soliton train. Well studied in hydrodynamics, particularly in the context of undular bores, collisionless plasma, and superfluids [4], dispersive shock waves have received less attention in optics. Here, we extend the studies of [3] to include the effects of a nonlocal nonlinearity. Experimentally and numerically, we find that nonlocality creates an effective damping force, inhibiting the shock speed and reducing oscillations by transferring momentum to larger scales.

Many optical materials respond nonlocally, in that the index of refraction at a particular location is determined by the intensity not only at that point, but also around that point in the material as well. The spatial extent of the index contribution at that point is assumed to be determined only by the properties of the medium itself. Nonlocal phenomena appear in many fields, such as plasma physics [5] and Bose–Einstein condensation (BEC) [6], and can arise in optics through physical processes such as atomic diffusion [7], photorefractive charge transport [8], interactions in liquid crystals [9], and thermal self-action [10,11]. Here, we use this last effect and consider the self-defocusing of cw spatial beams in a thermal liquid cell.

The spatial beam dynamics considered here is modeled accurately by the nonlinear Schrödinger equation:

$$i\frac{\partial\psi}{\partial z}+\frac{1}{2k_0}\nabla_\perp^2\psi+\Delta n(\rho)\psi=0, \tag{1}$$

where ψ is the slowly varying amplitude of the optical field, $k_0=2\pi n_0/\lambda$ is the wavenumber in a medium with the base index n_0, and Δn is the nonlinear index change induced by the intensity $\rho=|\psi|^2$. In many cases, a nonlocal nonlinearity can be modeled by a convolution operation: $\Delta n[\rho(\mathbf{r})]=\gamma\int R(\mathbf{r}')\rho(\mathbf{r}-\mathbf{r}')d\mathbf{r}'$, where $R(\mathbf{r}')$ is the medium's response function normalized to unity, i.e., $\int R(\mathbf{r}')d\mathbf{r}'=1$ [12], γ is the nonlinear coefficient, and the integration takes place over the transverse dimensions of the system. For the thermal medium considered below, we assume a Gaussian response function,

$$R(x)=(\pi w^2)^{-1/2}\exp(-x^2/w^2),$$

where w represents the effective range of the nonlocality.

To gain intuition on shock behavior, it is helpful to express Eq. (1) in a more hydrodynamic form. This is done via the Madelung transformation $\psi(x,z)=\sqrt{\rho(x,z)}\exp[iS(x,z)]$ [13], which, after scaling variables by k_0, yields two Euler-like fluid equations. In one dimension, these are

$$\frac{\partial\rho}{\partial z}+\frac{\partial}{\partial x}(\rho v)=0, \tag{2}$$

$$\frac{\partial v}{\partial z}+v\frac{\partial v}{\partial x}=\frac{\partial}{\partial x}[\Delta n'(|\psi|^2)]+\frac{1}{2}\frac{\partial}{\partial x}\left(\frac{1}{\sqrt{\rho}}\frac{\partial^2}{\partial x^2}\sqrt{\rho}\right), \tag{3}$$

where $v=\partial S/\partial x$ is the optical fluid velocity, $\rho=|\psi|^2$ is the fluid density/intensity, and $\Delta n'=\Delta n/k_0$. Equation (2) expresses conservation of power, while Eq. (3) is a momentum equation that states that optical flow results from nonlinear pressure and diffraction. We now consider a self-defocusing nonlinearity for which $\Delta n'<0$, so that regions of high intensity cause outward flow. The convective derivative implies that light waves will steepen as they propagate, eventually forming shocks. For a symmetric response function, such as the Gaussian considered here, there is no "viscosity" [even derivative in Eq. (3), e.g., $\partial^2 v/\partial x^2$] in the system. In this case, wave breaking is prevented by diffraction [last term in Eq. (3)], a nondissipative regularization that leads to an oscillatory wavefront.

Numerical simulations of dispersive/diffractive shock waves in a nonlocal nonlinear medium are shown in Fig. 1. The input intensity profile consists of a Gaussian hump on a constant, low-level background, and output profiles are shown as the nonlocal parameter w is increased. As in [3], the expanding wave consists of two repulsive humps whose fronts are characterized by oscillations. As the range of non-

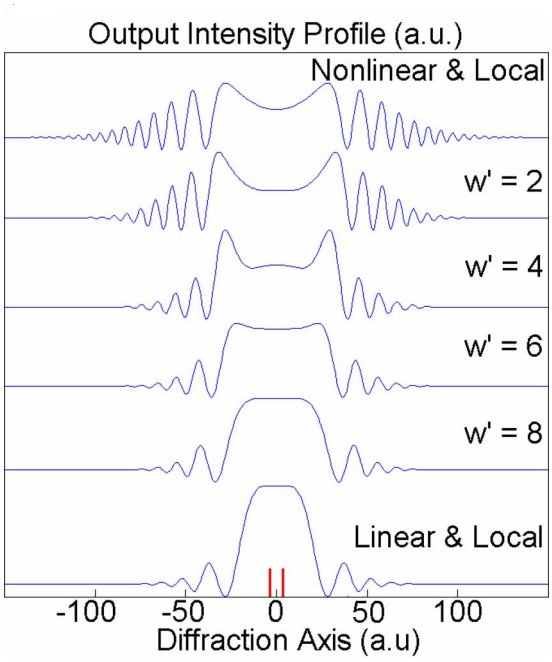

Fig. 1. (Color online) Numerical simulation of dispersive shock waves as a function of nonlocal response width (w', normalized to the width of the input Gaussian hump). The red bars on the x-axis indicate the FWHM of the initial hump, which has a 25:1 peak-to-background intensity ratio.

locality increases, the central region broadens and the oscillations in the tails become damped. Several limiting forms of the response function are useful to consider. In the limit of a delta-function response, the nonlinearity reduces to the local Kerr case $\Delta n = \gamma\rho$. (In this case, the background intensity defines an effective sound speed $c_s = \sqrt{|\gamma|\rho_\infty}$, so that the initial hump is automatically "supersonic" [3].) In the limit of a response width narrow compared to the input, the nonlinearity can be expanded in a Taylor series, giving $\Delta n = \gamma\rho + \gamma(\langle x^2\rangle/2)(\partial^2\rho/\partial x^2)$, where $\langle x^2\rangle = w^2/2$ is the average variance of the nonlocality. The second term has the same dispersive order as diffraction and has a spatially dependent effect, weakening the effective repulsive pressure in the central part of the Gaussian beam while enhancing it in the tails. In the opposite limit of response width much greater than input beam width, the response of the medium is equally strong across the entire beam profile; the hump does not experience a nonlinear phase shift relative to the background, and the overall response (nonlinearity plus nonlocality) approaches the linear, local case. Dynamically, though, higher-order terms and boundary effects arise in the longer-range limits, meaning that complex self-action and wave mixing are taking place [14,15].

Experimental measurements were made by projecting 532 nm laser light onto a 1 cm × 1 cm plastic cell containing ethanol doped with iodine. Physically, the iodine absorbs the green light and subsequently creates a thermal gradient in response to the light intensity. The heat diffuses throughout the cell and produces a nonlocal index of refraction via the thermo-optic effect: $\Delta n = (dn/dT)\Delta T$. Neglecting convection, the resulting system can be modeled by Eqs. (2) and (3). Following [3], we create a hump-on-background input profile by using a Mach–Zehnder interferometer and placing a spherical lens in one of the arms. Both beams are then recombined onto the input face of the cell, and the output face is imaged onto a CCD camera. In the liquid cell, the plane-wave background causes uniform heating and thus no relative index change, while the Gaussian hump produces a spatially dependent nonlinearity. The liquid medium responds to this profile in two different stages: relatively fast thermal diffusion followed by convection of the fluid itself (after ~0.5 s of cw heating). Measuring the output profile at different times

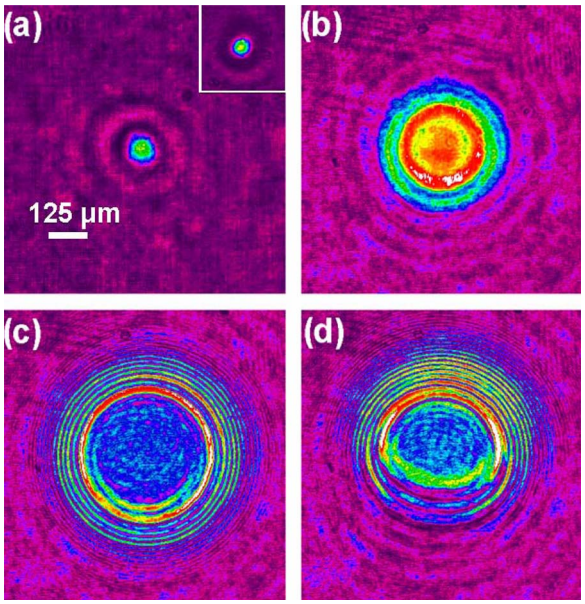

Fig. 2. (Color online) Experimental evolution of dispersive shock wave after 1 cm of propagation in an ethanol + iodine liquid cell. (a) Linear case. Inset, input profile. (b) Initial shock formation in nonlinear, nonlocal case. (c) Approximately 200 ms later, quasi-steady-state (before convection of fluid) shock profile. (d) Steady state, with asymmetry due to convection.

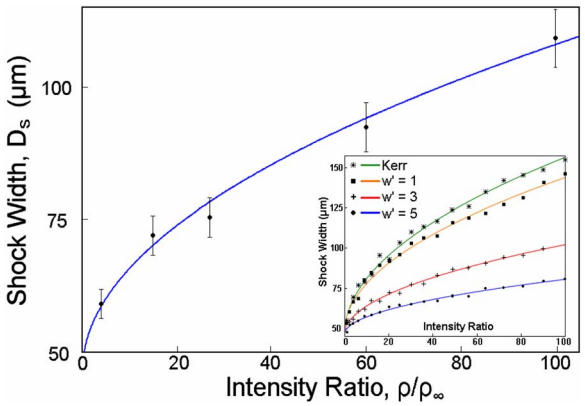

Fig. 3. (Color online) Shock length, measured horizontally from centerline to the end of oscillations, as a function of hump-to-background intensity ratio. Black dots, experimental measurements. Solid curve, best fit of $D_s = a_s(1 + b_s\sqrt{\rho/\rho_\infty})$, with $a_s = 46\ \mu$m and $b_s = 0.13$. Inset, numerical simulation, showing consistency of scaling relation as a function of nonlocal response width w'.

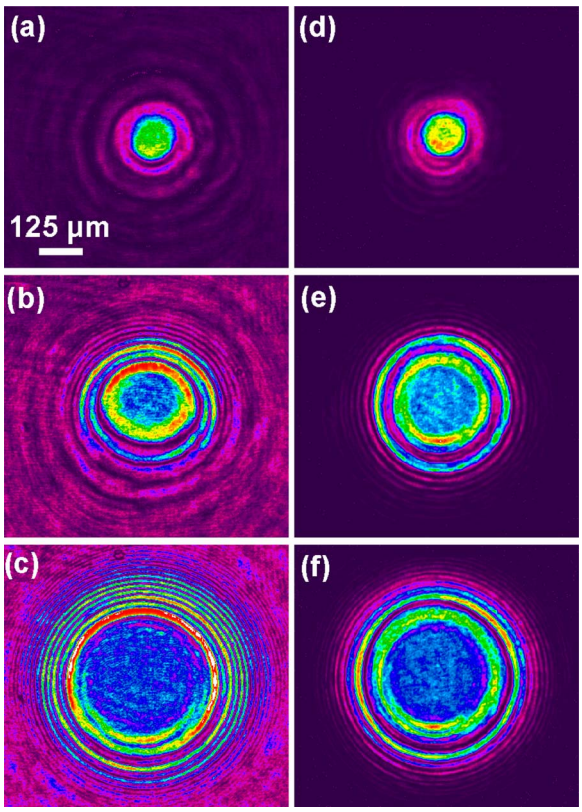

Fig. 4. (Color online) Comparison of shock profiles with background (a)–(c) and without background (d)–(f). From top to bottom, the laser power is 6.1, 24.4, and 36.6 mW, respectively.

allowed different stages of spreading (and thus nonlocality) to be observed. As the heating time increases, the output evolves from linear diffraction [Fig. 2(a)] to weak Fig. 2(b) and then strong [Fig. 2(c)] nonlocal shock behavior. For longer times, the shock begins to move vertically and develop an asymmetry [Fig. 2(d)], due to convection of the liquid medium itself.

As the hump-to-background ratio increases, the shocks become more violent, with faster oscillations (higher self-phase modulation) in the tails. Taking the shock width as a measure of its velocity (Fig. 3), it is found that the front speed increases with intensity ratio according to the relation $D_s = a_s(1 + b_s\sqrt{\rho/\rho_\infty})$, with fitting parameters $a_s = 46\ \mu$m and $b_s = 0.13$. This dimensional scaling follows from Eq. (3) and is the same as that observed in [3], but with a rate of increase much slower than in the local, Kerr case (Fig. 3, inset). For the liquid medium here, the b_s coefficient suggests a nonlocal response of roughly twice the width of the input hump.

Figure 4 shows the effects of the background intensity, obtained by measuring the output for different power levels both with (left column) and without (right column) the background. Each column shows the output profiles for input Gaussian powers of 6.1, 24.4, and 36.6 mW, respectively. Interestingly, even without the background, oscillations are still apparent in the output. Known as thermal blooming [10,11,16,17], this single-beam broadening has recently been interpreted in a shock context [18]. The shock waves observed here, however, differ from these more classical defocused waves in two ways: the central region is broad and flat, without an inner series of concentric circles, and the outer rings have a decreasing period with radial distance. This latter characteristic is a signature feature of dispersive shock waves [4] and results in our case from a steep initial gradient, forcing the initial Gaussian hump to wave break into its own tails.

In conclusion, dispersive optical shock waves have been characterized numerically and experimentally in a nonlinear, nonlocal medium. A hydrodynamic model was developed, showing that shock formation is inhibited by the nonlocal response. It was shown that nonlocality acts as a nonviscous damping force, reducing the shock speed and inhibiting oscillations in the front. The results extend traditional laser observations of thermal blooming and reinforce the interplay between optical systems and hydrodynamic flow.

This work was supported by the NSF and AFOSR. C. Barsi would like to thank the ARO for generous support through a NDSEG fellowship.

References

1. G. P. Agrawal, *Nonlinear Fiber Optics* (Academic, 2001).
2. J. M. Dudley, G. Genty, and S. Coen, Rev. Mod. Phys. **78**, 1135 (2006).
3. W. Wan, S. Jia, and J. W. Fleischer, Nat. Phys. **3**, 46 (2007).
4. V. I. Karpman, *Nonlinear Waves in Dispersive Media* (Pergamon, 1974).
5. A. Litvak, V. Mironov, G. Fraiman, and A. Yunakovskii, Sov. J. Plasma Phys. **1**, 31 (1975).
6. F. Dalfovo, S. Giorgini, L. P. Pitaevskii, and S. Stringari, Rev. Mod. Phys. **71**, 463 (1999).
7. D. Suter and T. Blasberg, Phys. Rev. A **48**, 4583 (1993).
8. M. Segev, B. Crosignani, A. Yariv, and B. Fischer, Phys. Rev. Lett. **68**, 923 (1992).
9. C. Conti, M. Peccianti, and G. Assanto, Phys. Rev. Lett. **91**, 073901 (2003).
10. J. P. Gordon, R. C. C. Leite, R. S. Moore, S. P. S. Porto, and J. R. Whinnery, J. Appl. Phys. **36**, 3 (1965).
11. S. A. Akhmanov, D. P. Krindach, A. V. Migulin, A. P. Sukhorukov, and R. V. Khokhlov, IEEE J. Quantum Electron. **QE-4**, 568 (1968).
12. W. Krolikowski, O. Bang, J. J. Rasmussen, and J. Wyller, Phys. Rev. E **64**, 016612 (2001).
13. E. Madelung, Z. Phys. **40**, 322 (1927).
14. C. Rotschild, O. Cohen, O. Manela, M. Segev, and T. Carmon, Phys. Rev. Lett. **95**, 213904 (2005).
15. C. Rotschild, B. Alfassi, O. Cohen, and M. Segev, Nat. Phys. **2**, 769 (2006).
16. E. A. Mclean, L. Sica, and A. J. Glass, Appl. Phys. Lett. **13**, 369 (1968).
17. P. M. Livingston, Appl. Opt. **10**, 426 (1971).
18. N. Ghofraniha, C. Conti, G. Ruocco, and S. Trillo, Phys. Rev. Lett. **99**, 043903 (2007).